J Mater Sci: Mater Electron (2015) 26:3797–3804
DOI 10.1007/s10854-015-2905-7

# Structural, dielectric and electrical properties of the $Ba_2BiNbO_6$ double perovskite

**Niranjan Panda · B. N. Parida · R. Padhee · R. N. P. Choudhary**

Received: 8 December 2014 / Accepted: 1 March 2015 / Published online: 6 March 2015


**Abstract** The polycrystalline sample of $Ba_2BiNbO_6$ (a member of double perovskite family) was synthesized by a high-temperature solid-state reaction method (calcination at 910 °C, and sintering at 950 °C). Preliminary analysis of room temperature X-ray data pattern of the sample confirms the formation of a single phase compound in orthorhombic crystal system. The room temperature scanning electron microscope image of the pellet sample clearly shows the uniform distribution of grains and formation of a high density sample. Detailed studies of dielectric and polarization characteristics with temperature confirmed the existence of ferroelectricity in the material. Studies of electrical properties exhibits a strong correlation with the micro-structure and resistive properties of the material. The electrical transport shows the existence of non-exponential-type of conductivity relaxation in the material. This lead-free ferroelectric has many interesting characteristics as compared to that of their lead-based counterpart, $Pb_2BiNbO_6$.

## 1 Introduction

Most of the ferroelectric oxides have $BO_6$ oxygen octahedra, even though they have different crystal structures, electrical and mechanical properties, transition temperature ($T_c$) and remnant polarization ($P_r$) [1]. There are four different types of structures of ferroelectric oxides with oxygen octahedra namely; perovskite, tungsten-bronze, layer and pyrochlore. For the last few decades, there has been extensive investigation on ferroelectric oxides particularly on oxygen octahedral type because of various industrial and technological applications. Although a number of TB-type (complex perovskite) ferroelectrics have been studied, a lot of interest has been paid on ferroelectric niobates and tantalates for their electro-optic and other related applications. The first reported ferroelectric compounds of TB-type complex perovskite structure are lead metaniobate $PbNb_2O_6$ [2, 3] and lead metatantalate $PbTa_2O_6$ [4]. The transition temperature of these two compounds was reported to be 575 and 260 °C respectively. After the discovery of ferroelectricity in these two compounds, lots of compounds of the family were studied because of their many interesting properties useful for devices. Interestingly, single crystal or ceramic sample of lead barium niobate (PBN) shows high dielectric constant, pyroelectric, piezo-electric and electro-optic coefficients which are useful for many devices such as surface acoustic wave (SAW), pyroelectric and memory devices around the morphotoric phase boundary (MPB) [5–10]. The TB-type double perovskites with general formula $A_2BB'O_6$, (with, A = an alkaline earth, B and B′ are transition metals) have been studied because of their attractive physical properties [11], which depend on structural distortions and the characteristic properties of B and B′ cations. This chemical configuration results in a lot of opportunities to combine different elements of the periodic table, generating the possibility of synthesizing new materials. The $BaTiO_3$ which is simple perovskite is well known because of its ferroelectric character [12]. Partial substitutions of Ti by the Zr cation have been done by many authors, showing the

N. Panda
Department of Physics, PKACE, Bargarh 768028, Odisha, India

B. N. Parida (✉) · R. Padhee · R. N. P. Choudhary
Multifunctional Materials Research Laboratory, Department of Physics, Institute of Technical Education and Research, Siksha O Anusandahan University, Khandagiri, Bhubaneswar 751030, Odisha, India
e-mail: bichitra72@gmail.com

evolution of the electric behavior from a ferroelectric response for low concentration of Zr, to a ferroelectric relaxor [13] and a dielectric behavior for high concentrations of Zr [14]. However, the position of the substitutive cations in the crystallographic cell of the material is not usually reported. Location of all ions in the lattice is important for inferring the possibility of obtaining spontaneous polarization, in order to give rise to ferroelectric behavior. In the case of polycrystalline samples, the ferroelectric behavior depends greatly on the grain size, because the effects of imperfection frequently dominate the ferroelectric response of small grains, where a significant fraction of the material volume may be influenced by grain boundaries. It is known that cationic disorder produces substantial changes of the ferroelectricity of complex perovskites [15].

Nowadays, attempts are being made to keep the environment eco-friendly and free from toxic materials such as lead. There are a good number of lead-based ferroelectrics namely, PZT, PMN, PFN etc., which are having much superior quality as compared to that of non-ferroelectrics, are widely used for various types of sensors. Therefore, it is impossible to replace the above lead based compound completely; however, continuous efforts are being made to search for new lead-free ferroelectrics with comparable characteristics for the desired purpose. In view of this we have a synthesized lead-free tungsten bronze compound with chemical formula $Ba_2BiNbO_6$ by mixed oxide route, and studied its ferroelectric and electrical characteristics for possible devices.

## 2 Experimental

### 2.1 Sample preparation

The polycrystalline samples of $Ba_2BiNbO_6$ (BBN) were synthesized by a high-temperature mixed oxide route using high-purity (AR grade) ingredients: $BaCO_3$, $Bi_2O_3$, and $Nb_2O_5$ (>99 %, M/s LOBA Chemie Pvt. Ltd. India) as per the required stoichiometric proportions. The oxides and carbonate with the following composition were mixed in dry (air) and wet (methanol) medium for 3 h in agate mortar. Based on the repeated firing and grinding at different high temperatures (close to melting/decomposition temperature of ingredients) the calcinations temperature for formation of the material ($Ba_2BiNbO_6$) was decided. Finally the material was calcined at 910 °C for 4 h.

$$2\ BaCO_3 + 0.5Bi_2O_3 + 0.5Nb_2O_5 \rightarrow\ Ba_2BiNbO_6 + CO_2$$

The calcined fine powder of the material was then cold pressed into the form of cylindrical pellets of diameter 10 and 1–2 mm thickness under a uniaxial pressure of $4 \times 10^6$ $nm^{-2}$ using a hydraulic press. Polyvinyl alcohol (PVA) was used as a binder to prepare pellets. The pellets were then sintered at an optimized temperature of 925 °C (based on repeated firing) in air atmosphere for 4 h.

### 2.2 Characterization techniques

An X-ray diffraction (XRD) pattern data of calcined powder was recorded at room temperature using X-ray powder diffractometer (PAN Analytical XPERT) with $CuK_\alpha$ radiation ($\lambda = 1.5405$ Å) in a wide range of Bragg's angle ($\theta$) ($20° \leq 2\theta \leq 80°$) at a scanning rate of 2°/min. The sintered pellets were electroded with high-quality silver paste, and dried at 150 °C for 4 h before taking dielectric and electrical measurements. The microstructures of the pellet samples were recorded by Jeol JSM-6480 LV SEM at room temperature. Compositional analysis of the pellet sample was carried out by the energy dispersive X-ray spectroscopy (EDS) attached with the SEM of above model.

The dielectric (capacitance, dissipative factor), impedance and inductance parameters of the sintered pellet were measured as a function of frequency (1 kHz–1 MHz) at different temperatures (25–500 °C) using a computer-controlled phase sensitive meter (PSM 1735 LCR 4NL, UK) with a laboratory-designed and fabricated sample holder and furnace. A chromel–alumel thermo-couple and Rishab digital milli-voltmeter were used to record the temperatures. The polarization (hysteresis loop) of the material on the poled sample (electric field = 6 kV/cm, time = 8 h) was obtained at different temperatures using hysteresis loop tracer (M/S Marine India, New Delhi).

## 3 Results and discussion

### 3.1 Structural study

Figure 1 shows the room temperature XRD pattern of $Ba_2BiNbO_6$. The diffraction pattern of the compound consists of sharp and single diffraction peaks, which are different from that of the ingredients of the prepared compounds confirming the formation of a single-phase new compound [16]. As most of tungsten bronze structure has tetragonal or orthorhombic structure, all the observed peaks of the pattern were indexed in these crystal systems with different unit cell configurations using a standard computer program package "POWD" [17]. On the basis of best agreement between observed and calculated inter planar spacing (d), an orthorhombic unit cell was selected. The selected unit cell parameters of the sample (as given in the figure) were refined using least-squares refinement subroutine of the above computer program. The estimated standard deviation of cell parameters was 0.0018 Å. These

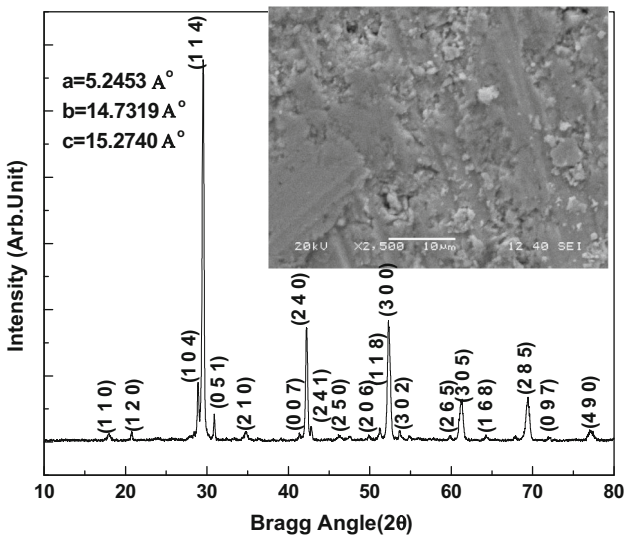


**Fig. 1** Shows room temperature XRD pattern and SEM micrograph of BBN

values are found to be very much consistent with those of some reported compounds of similar structure [18].

The scattered crystallite or particle size (P) of the compound was calculated using the broadening of some widely spread (over Bragg angles) strong and medium reflections in the Scherrer's equation: $P_{hkl} = \frac{k\lambda}{\beta_{1/2}\cos\theta_{hkl}}$ [19], where k (constant) = 0.89, $\lambda = 1.5405$ Å and $\beta_{1/2}$ = full width at half maximum (in radians). The average value of $P_{hkl}$ is found to be 28 nm.

Figure 1(inset) shows the surface morphology of BBN recorded on the gold plated bulk pellet sample using a SEM. The nature and size of the microstructures of the sample suggest that surface is highly dense due to uniformly distribution of grains. In spite of sintering at optimized high temperature some small voids of irregular shape and dimension are seen in the compound. The calculated relative density of the sintered pellet is 5.85.

The elemental identification of the composites was done with EDX technique. The EDX spectra of the composites are shown in Fig. 2. The absence of extra elements other than expected (Ba, Bi, Nb and O) in the EDX spectra reveals the purity of the sample and confirms the formation of single phase i.e., orthorhombic double perovskite structure of ferroelectric phase in the compound.

### 3.2 Dielectric study

The temperature variation of relative dielectric constant ($\varepsilon_r$) and tangent loss (tanδ) at different frequencies (1, 10, 100 kHz and 1 MHz) of the sample are shown in Fig. 3. It is noticed that $\varepsilon_r$ increases up to a temperature (referred as transition temperature ($T_c \sim 350$ °C)), and then it decreases suggesting ferroelectric-paraelectric phase transition at this temperature. The temperature variations of tan δ at different frequencies also follow the similar pattern. The room temperature $\varepsilon_r$ and tan δ for BBN are 812 and 0.0219 respectively. The higher and smaller values of $\varepsilon_r$ and tan δ of BBN respectively at room temperature, are useful for capacitors, transducer and microwave applications. The increase in $\varepsilon_r$ can be ascribed to the electron–phonon interaction which is mainly observed in niobates. Above 430 °C, the increase in $\varepsilon_r$ can be ascribed to the thermally activated transport of space charges [20]. The higher value of $\varepsilon_r$ at lower frequency (1 kHz) of the compound is due the charge accumulation at grain boundaries [21]. Above $T_c$ there is monotonous increase in tan δ value which can be attributed to thermal transport of oxygen vacancies, $Bi^{+3}$ and $Nb^{+4}$ ions which act as donor centers initiating extrinsic n-type conduction in compound. A sharp increase in tan δ at higher temperature may be due to scattering of thermally activated charge carriers and some defects in the compound. At higher temperatures the conductivity begins to dominate, which in turn, is responsible for rise in tan δ. Also, at higher temperatures the contributions of ferroelectric domain walls to tan δ is less, which causes the rise in value of tan δ [22]. The nature of frequency dependence of dielectric parameters of the material can be explained by the Maxwell–Wagner and Koop's phenomenological models [23]. As per this model, dielectric medium contains highly conducting grains and poorly conducting grain boundaries. At higher frequencies the grain are more effective while the grain boundaries are found to be more effective at lower frequencies and higher temperatures. The decreasing nature of $\varepsilon_r$ on increasing frequency may be considered due to the electron hopping between $Nb^{+5}$ and $Nb^{+4}$ at octahedral sites which cannot follow the alteration of ac electric field at higher frequencies. Therefore, electrons have to pass through the well conducting grains and the poorly conducting grain boundaries. As the grain boundaries have large resistance, the electrons pile up there, and produce large space charge polarization. Therefore, $\varepsilon_r$ has larger value in the low-frequency range. On further increase of frequency, the electrons change their direction of motion rapidly, which hinders the movement of electrons inside the dielectric material and thus accumulation of charges at the grain boundaries decreases resulting in the decrease of $\varepsilon_r$.

### 3.3 Polarization study

Figure 4 shows hysteresis loop of the sample at two different temperatures. The remnant polarization ($2P_r$) of the compound at 30 and 50 °C was found to be 5.74 and 5.12 μC/cm$^2$ respectively. The coercive field ($2E_c$) at these temperatures was found to be 0.11 and 0.1 kV/cm respectively. It is observed that the value of remnant

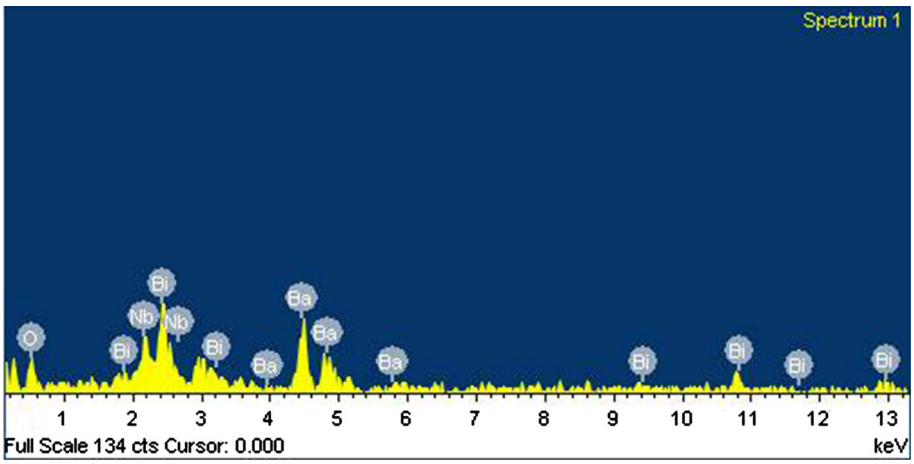


**Fig. 2** EDX of the pellet sample BBN

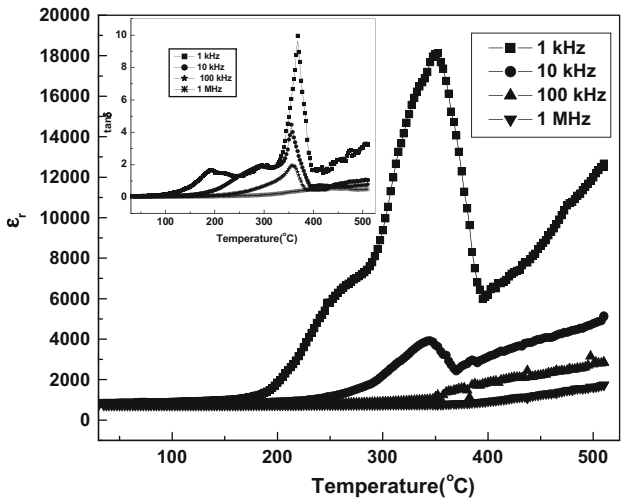


**Fig. 3** Shows the temperature variation of $\varepsilon_r$ and tanδ BBN at different frequency

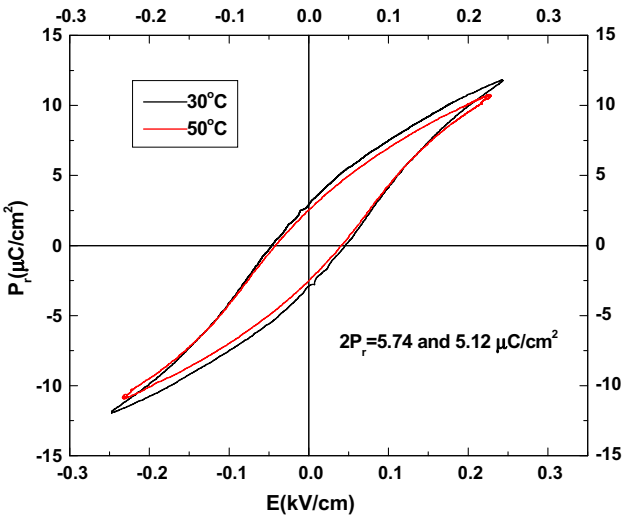


**Fig. 4** Shows temperature variation PE loop of BBN

polarization and coercive field decreases with rise in temperature. Again, the area of the room temperature loop was found to be decreased with rise in temperature which confirms the existence of ferroelectric properties in the material.

### 3.4 Impedance and modulus spectroscopy

Complex impedance spectroscopy (CIS) technique is widely used to study frequency-temperature dependence of the electrical properties of dielectrics and ionic conductors. By using this technique, one can able to distinguish (1) bulk, (2) grain boundary and (3) electrode polarization effect of the material. When an ac signal is applied across the pellet sample, its output response is measured. The impedance measurements of the materials give us data having both real (resistive) and imaginary (reactive) components. For this purpose some basic equations/formulism of impedance and electrical modulus are used in this technique such as: complex impedance $Z^* = Z' + jZ''$, complex modulus $\frac{1}{\varepsilon^*} = M^* = M' + jM'' = j\omega C_o Z^*$, and complex permittivity $\varepsilon^* = \varepsilon' - j\varepsilon''$. Using above equations we will get following impedance and modulus formalism to calculate and study the detail electrical properties of the materials.

$Z^2 = Z'^2 + Z''^2$, $M' = -\omega C_o Z'', M'' = \omega C_o Z'$ where $C_o$ is the geometrical capacitance, $j = \sqrt{-1}$.

#### *3.4.1 Impedance analysis*

Figure 5 shows variation of $Z' \sim Z''$ (Nyquist plot) at different temperature of sample BBN. All the semicircles exhibit some depression instead of a semicircle centered on the real axis. This behavior is indicative of non-Debye type of relaxation and it also manifests that there is a distribution of relaxation time instead of a single relaxation time in

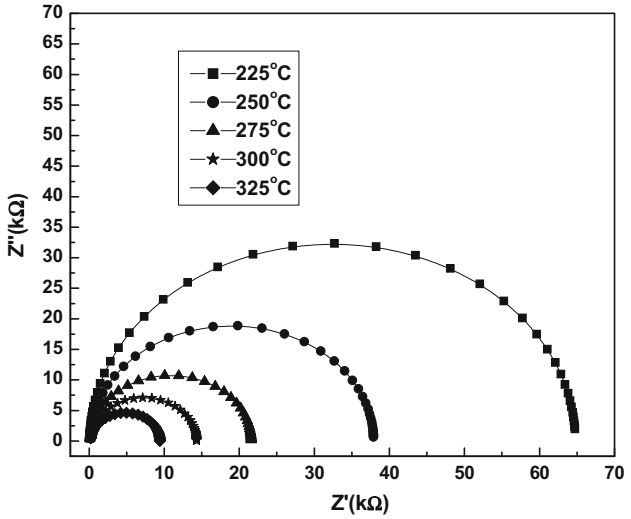


**Fig. 5** Shows variation of $Z' \sim Z''$ (Nyquist plot) at different temperature of BBN

the studied material. The value of bulk resistance ($R_b$) at different temperatures has been obtained from the intercept of the semicircular arcs on the real axis ($Z'$). It clearly shows that the parameters $R_b$ decreases with rise in temperature suggesting the NTCR behavior of the material. In an ideal Debye like response, a perfect semi-circle with its center at $Z'$ axis is observed for which equivalent circuit to fit the experimental data is parallel combinations of (CR). Since semicircles in the studied material at different temperature are depressed type suggesting non-Debye type of relaxations, for which we have number of relaxation time instead of single relaxation time.

Figure 6 shows the variation of $Z''$ with frequency at selected temperatures. It is observed that the value of $Z''$ decreases with rise in frequency as well as temperature in the sample. The value of $Z''$ increases with rise of frequency and attains a maximum at certain frequency ($Z''_{max}$). This is due to the presence of relaxation in the sample [20]. The frequency at which $Z''$ attains maximum value is known as relaxation frequency ($f_r$). Inverse of $f_r$ is known as relaxation time of the sample. Again, relaxation time decreases with rise in temperature suggesting the temperature dependence of relaxation phenomena. Generally, in dielectric material relaxation process occurs due to the presence of immobile charges at low temperatures and defects/vacancies at higher temperatures [24].

### 3.4.2 *Modulus analysis*

The analysis of electrical modulus, measured from impedance analyzer or LCR meter, is very useful to detect parameters such as electrode polarization, grain boundary conduction effect, bulk properties electrical conductivity and relaxation time. Figure 7 shows the variation of $M''$ with frequency at selected temperatures. Once again, $M''$ spectroscopy studies provide nature of relaxation phenomena in the material. The peak or maximum value of $M''$ ($M''_{max}$) shifts to higher frequency side which suggests the existence of hopping mechanism in which charge carriers dominates intrinsically and hence mechanism is considered as thermally activated process. Asymmetric broadening of the peaks indicates spread of relaxation with different time constants, which once again suggests non- Debye type [15].

The reactive part of impedance ($Z''$) and modulus ($M''$) spectroscopy plot is shown in Fig. 8. Sinclair et al. [25] reported that the combine plot of $Z''$ and $M''$ as a function of frequency is used to detect the presence of smallest capacitance and largest resistance. According to them, if

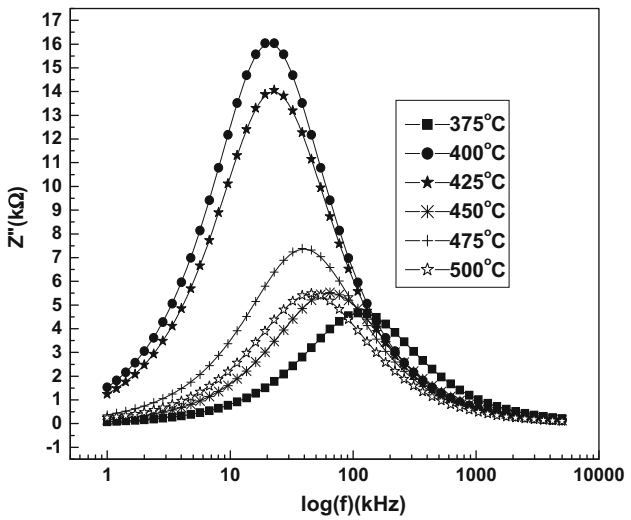


**Fig. 6** Shows frequency dependent $Z''$ at different temperature of BBN

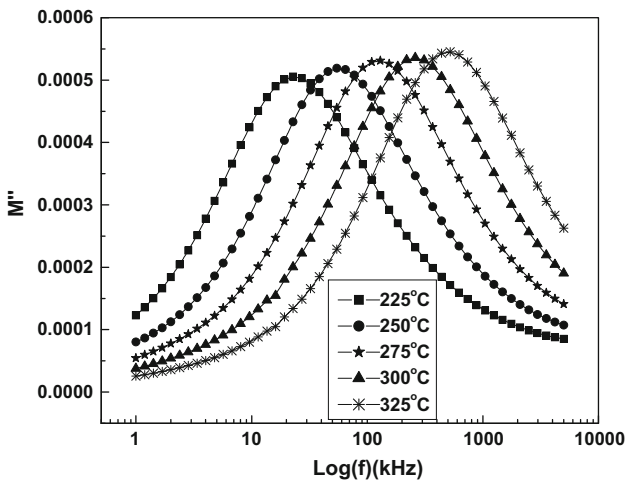


**Fig. 7** Shows frequency dependent $M''$ at different temperature of BBN

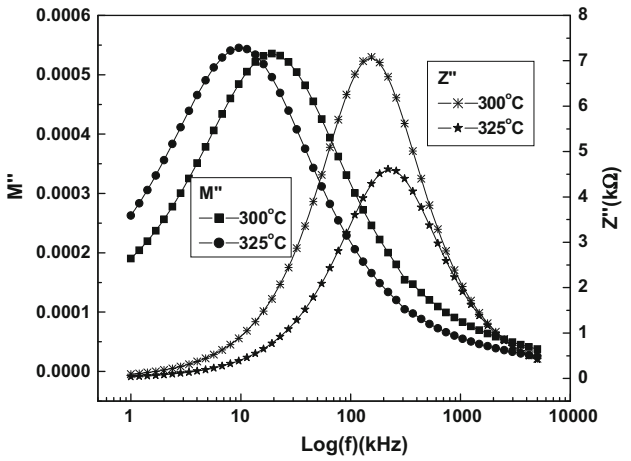


**Fig. 8** Shows combine plot of Z″ and M″ with frequency at different temperature

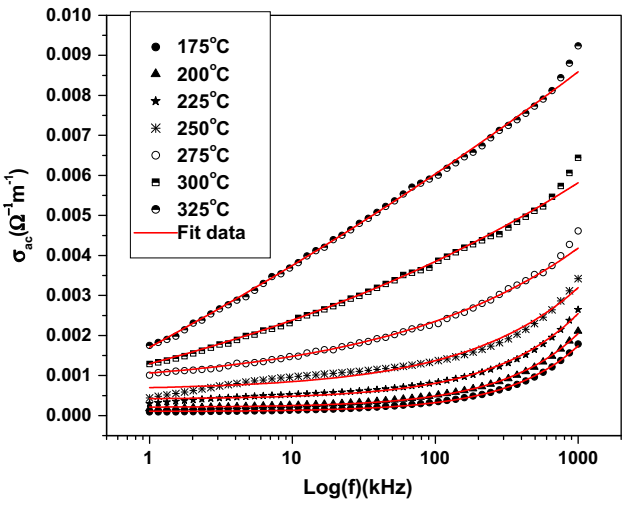


**Fig. 9** Shows frequency dependent ac conductivity at different temperature of BBN

peaks of Z″ and M″ ~ frequency are occur at different frequencies then motion of charge carrier is short range whereas for long range movement of charge carrier peaks are occur at same frequencies. In the studied compound there is mismatch of peaks at fixed temperatures suggesting short range motion of charge carriers and departure from ideal Debye-like behaviour [26].

## 3.5 Conductivity study

### *3.5.1 Ac conductivity*

Studies of frequency-temperature dependence of ac conductivity are generally carried out to understand the type of electrical conduction mechanism and the nature of charge carriers in the material. The ac electrical conductivity ($\sigma_{ac}$) is calculated using an empirical relation, $\sigma_{ac} = \omega\varepsilon_r\varepsilon_0 \tan\delta$, where $\varepsilon_0$ is permittivity in free space and $\omega$ is angular frequency. To understand the effect of frequency on conduction mechanism of the material, we have to use Jonscher's universal power law [27]: $\sigma_T(\omega) = \sigma(0) + \sigma_1(\omega) = \sigma_0 + A\omega^n$ where $\sigma$ (0) is the frequency independent term giving rise to dc conductivity and $\sigma_1(\omega)$ is the purely dispersive component of ac conductivity. The exponent n can have a value between zero and one which represents the degree of interaction between mobile ions and lattices around them whereas A determines the strength of polarizability.

Figure 9 shows the variation of $\sigma_{ac}$ of the material with frequency at different temperatures. At higher temperatures the conductivity curves show frequency independent plateau in the low-frequency region whereas at higher frequencies $\sigma_{ac} \alpha \omega^n$, thus frequency dispersion is still maintained in the material. It is obvious that $\sigma_{ac}$ increases with rise in frequency but it is nearly independent at low frequency. Therefore, extrapolation of this part towards lower frequency side gives $\sigma_{dc}$. The increasing trend of $\sigma_{ac}$ with rise in frequency may be attributed to the disordering of cations between neighboring sites, and presence of space charges [28]. In the high frequency region the curves approach to each other. The nature of conductivity plots reveals that the curves exhibit low frequency dispersion phenomena obeying the Jonscher's power law. According to Jonscher [27], the origin of the frequency dependence of conductivity lies in the relaxation phenomena arising due to mobile charge carriers. When a mobile charge carrier hops to a new site from its original position, it remains in a state of displacement between two potential energy minima obeying above power law. The value of $n < 1$ signifies that the hopping motion involves a translational motion with a sudden hopping whereas $n > 1$ means that the motion involves localized hopping without the species leaving the neighborhood. The frequency at which change in slope takes place is known as hopping frequency of the polarons ($\omega_p$), and is temperature dependent. The material obeys universal power law which is confirmed by a fit of above equation to the experimental data (Fig. 9) where solid line correspondence to fitted curve and symbols are experimental data. From non-linear fitting it is found that the motion of charge carriers in the samples is translational one because of small value of n (<1). A close look on the plot reveals value of conductivity increases with increase of temperature once again supports the NTCR behavior of the sample.

Figure 10 shows the variation of fitting parameter A and n with temperature. It is seen that the value of n decreases with rise in temperature and becomes minimum near $T_c$ in BBN. Again, it increases with increase in temperature whereas pre-exponential factor A has a reverse trend. The

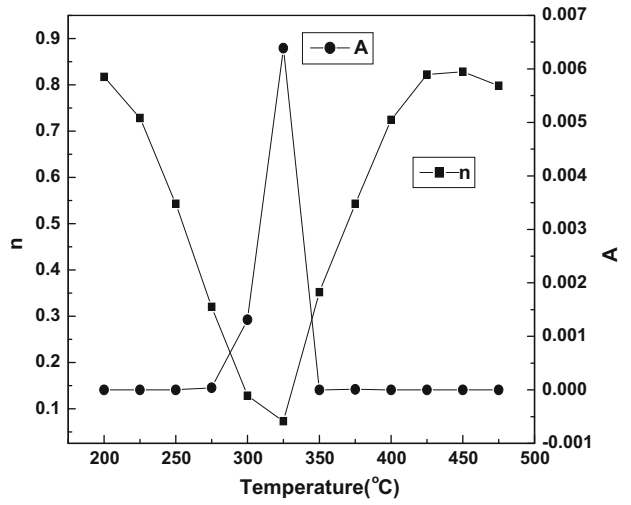


**Fig. 10** Shows variation of fitting parameter A and n with the temperature of BBN

exponent n represents interaction between mobile ions with the lattice around them. The observed minima at $T_c$ (or decreasing trend with temperature) suggest a strong interaction between the lattice and mobile ions. According to dynamic theory [29, 30], one of the transverse optical mode (soft mode) is weakened, and the restoring force tends to be zero at transition temperature $T_c$. Therefore, if charge carriers coupled with soft mode, they become mobile at $T_c$, and thus conductivity increases. The pre-exponential factor A determines the strength of polarizability. The maximum value of A at $T_c$ suggests the presence of high polarizability i.e., maximum dielectric constant.

### *3.5.2 dc conductivity*

Figure 11 shows variation of $\sigma_{dc} \sim 10^3/T$ for the compound. The nature of the plot follows the Arrhenius relation

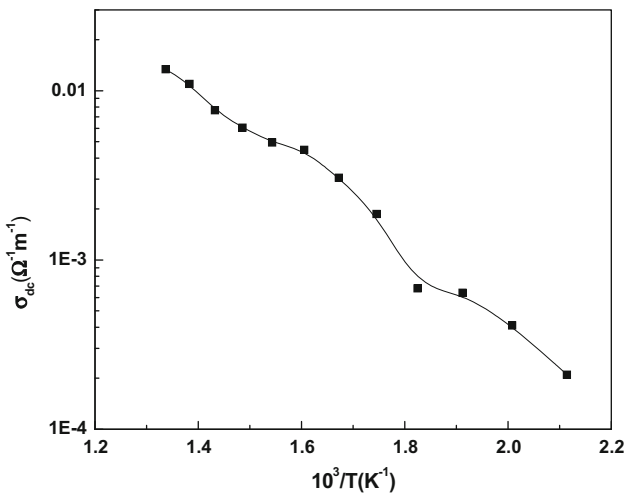


**Fig. 11** Shows variation of $\sigma_{dc}$ with the reciprocal of absolute temperature of BBN

$\sigma_{dc} = \sigma_o e^{\frac{-E_a}{K_B T}}$ [19]. The calculated activation energy ($E_a$) is 0.846 eV for BBN. Conductivity increases with rise of temperature signifying NTCR behavior in the studied compound.

## 4 Conclusion

The preliminary structural analysis of synthesized material using X-ray diffraction data shows that the material has an orthorhombic crystal structure. Detailed studies of temperature dependence of dielectric and electric polarization conclude that the material has ferroelectric characteristics. Impedance spectroscopy studies indicate that the material exhibits (1) conduction due to bulk (grain) effect, (2) NTCR-type behavior and (3) temperature dependent relaxation phenomena. Modulus analysis indicates non–exponential type of conductivity relaxation in the material. Ac conductivity study reveals the material is semiconducting nature and obeys Jonscher's universal power law.

## References

1. F.W. Aiger, *Modern Oxide Materials-Preparation, Properties and Device Applications* (Academic Press. Inc., London, 1972)
2. G. Goodman, Ferroelectric properties of lead metaniobate. J. Am. Ceram. Soc. **36**, 368–372 (1953)
3. M.H. Francombe, B. Lewis, Structural, dielectric and optical properties of ferroelectric lead metaniobate. Acta Crystallogr. **11**, 696 (1958)
4. M.E. Lines, A.M. Glass, *Principles and applications of ferroelectrics and related materials* (Oxford University Press, Oxford, UK, 2001)
5. C.A. Randall, A.D. Hilton, D.J. Barber, T.R. Shrout, Extrinsic contributions to the grain size dependence of relaxor ferroelectric $Pb(Mg_{1/3}Nb_{2/3})O_3$: $PbTiO_3$ ceramics. J. Mat. Res. **8**, 880–884 (1993)
6. R. Guo, A.S. Bhalla, C.A. Randall, L.E. Cross, Dielectric and pyroelectric properties of the morphotropic phase boundary lead barium niobate (PBN) single crystals at low temperature (10–300 K). J. Appl. Phys. **67**, 6405 (1990)
7. M. Lee, R.S. Feigelson, A. Liu, L. Hesselink, Photorefractive properties of tungsten bronze ferroelectric lead barium niobate ($Pb_{1-x}Ba_xNb_2O_6$)crystals. J. Appl. Phys. **83**, 5967 (1998)
8. T.R. Shrout, H. Chen, L.E. Cross, Dielectric and piezoelectric properties of $Pb_{1-x}Ba_xNb_2O_6$ ferroelectric tungsten bronze crystals. Ferroelectrics **74**, 317–324 (1987)
9. M. Lee, H. Lee, R.K. Route, R.S. Feigelson, Optical properties of lead barium niobate ($Pb_{1-x}Ba_xNb_2O_6$) crystals. J. Appl. Phys. **81**, 917 (1997)
10. G. Burns, F.H. Dacol, R. Guo, A.S. Bhalla, Ferroelectric (Pb, Ba)$Nb_2O_6$ near the morphotropic phase boundary. Appl. Phys. Lett. **57**, 543 (1990)
11. V.R. Palkar, S.K. Malik, Observation of magnetoelectric behavior at room temperature in $Pb(Fe_xTi_{1-x})O_3$. Solid State Commun. **134**, 783–786 (2005)
12. D.A. Landínez Téllez, G. Peña Rodríguez, J. Arbey Rodríguez, F. Fajardo, J. Roa Rojas, Structural, magnetic, multiferroic, and

electronic properties of $Sr_2TiMnO_6$ double perovskite. Dyna **79**, 111–115 (2012)
13. V.A. Isupov, Nature of physical phenomena in ferroelectric relaxors. Phys. Solid State **45**, 1107–1111 (2003)
14. P. Baettig, N.A. Spaldin, Ab initio prediction of a multiferroic with large polarization. Appl. Phys. Lett. **86**, 12505–12507 (2005)
15. C. Ang, R. Guo, A.S. Bhalla, L.E. Cross, Dielectric dispersion at microwave frequencies. J. Appl. Phys. **87**, 3937–3940 (2000)
16. H.P. Klug, L.E. Alexander, *X-ray Diffraction Procedures for Polycrystalline and Amorphous Materials* (Wiley-Interscience, New York, 1974)
17. E.W. POWD, *An interactive powder diffraction data interpretation and indexing Program*, *Ver 2.1* (School of Physical Science, Finders University of South Australia, Bedford Park, SA 5042, Australia)
18. B.N. Parida, P.R. Das, R. Padhee, R.N.P. Choudhary, A new ferroelectric oxide $Li_2Pb_2Pr_2W_2Ti_4Nb_4O_{30}$: synthesis and characterization. J. Phys. Chem. Solids **73**, 713 (2012)
19. B.D. Cullity, *Elements of X-ray Diffraction* (Addison-Wesley Publishing Co. Inc., Boston, 1978)
20. B.N. Parida, P.R. Das, R. Padhee, R.N.P. Choudhary, Phase transition and conduction mechanism of rare earth based tungsten-bronze compounds. J. Alloys Compd. **540**, 267 (2012)
21. K. Jawahar, Choudhary RNP, structural and dielectric properties of $Y_{3/2}Bi_{3/2}Fe_5O_{12}$. Mater. Lett. **62**, 911–913 (2008)
22. P.R. Das, L. Biswal, B. Behera, R.N.P. Choudhary, Structural and electrical properties of $Na_2Pb_2Eu_2W_2Ti_4X_4O_{30}$ (X = Nb, Ta) ferroelectric ceramics. Mater. Res. Bull. **44**, 1214–1218 (2009)
23. C.G. Koops, On the dispersion of resistivity and dielectric constant of some semiconductors at audiofrequencies. Phys. Rev. **83**, 121–124 (1951)
24. D.P. Almond, A.R. West, Impedance and modulus spectroscopy of "real" dispersive conductors. Solid State Ionics **11**, 57–64 (1983)
25. D.C. Sinclair, A.R. West, Impedance and modulus spectroscopy of semiconducting $BaTiO_3$ showing positive temperature coefficient of resistance. J. Appl. Phys. **66**, 3850 (1989)
26. M. Nobre, S. Lanfredi, Ferroelectric state analysis in grain boundary of $Na_{0.85}Li_{0.15}NbO_3$ ceramic. J. Appl. Phys. **93**, 5557 (2003)
27. A.K. Jonscher, Nature **267**, 673 (1977)
28. N.K. Karan, D.K. Pradhan, R. Thomas, B. Natesan, R.S. Katiyar, Solid State Ionics **179**, 689 (2008)
29. Z. Lu, J.P. Bonnet, J. Ravez, P. Hagenmuller, Solid State Ionics **57**, 235 (1992)
30. A.K. Jonscher, *Dielectric Relaxation in Solids* (Chelsea Dielectric Press, London, 1983)